

Review

Targeted Contrast Agents for Molecular MRI

Sara Lacerda 

Centre de Biophysique Moléculaire, Rue Charles Sadron, 45071 Orléans CEDEX 2, France; sara.lacerda@cnr.fr; Tel.: +33-2-3825-5604

Received: 8 November 2018; Accepted: 30 November 2018; Published: 4 December 2018



Abstract: Molecular magnetic resonance imaging (MRI) provides information non-invasively at cellular and molecular levels, for both early diagnosis and monitoring therapeutic follow-up. This imaging technique requires the development of a new class of contrast agents, which signal changes (typically becomes enhanced) when in presence of the cellular or molecular process to be evaluated. Even if molecular MRI has had a prominent role in the advances in medicine over the past two decades, the large majority of the developed probes to date are still in preclinical level, or eventually in phase I or II clinical trials. The development of novel imaging probes is an emergent active research domain. This review focuses on gadolinium-based specific-targeted contrast agents, providing rational design considerations and examples of the strategies recently reported in the literature.

Keywords: MRI; molecular imaging; targeted contrast agent; lanthanide; protein-based contrast agent

1. Introduction

Molecular imaging offers the capacity of detecting and following-up events of processes happening at cellular and molecular levels that are signature (biomarkers) of early stages of a disease. Such medical exams require the use of a contrast agent (CA) that is specific to the event or process to detect, or which signal depends on the later.

Molecular magnetic resonance imaging (MRI) is a powerful non-invasive imaging technique which takes advantage of a very high spatial and temporal resolution and can provide detailed molecular/cellular information when combined with a contrast agent (to over-cross the lack of sensitivity inherent to MRI, see below). The MRI CA are molecules or particles that influence the relaxation of water protons. They can be T_1 -(positive) or T_2 -(negative) weighted, affecting the longitudinal or transverse relaxation times respectively. T_1 -weighted CA are mostly small gadolinium (Gd^{3+}) or manganese (Mn^{2+}) paramagnetic complexes, while the majority of the T_2 -weighted ones are iron oxide-based superparamagnetic nanoparticles. This review will focus on Gd^{3+} -based small molecule contrast agents.

MRI is widely used in clinics, with more than 30% of the exams made with the help of a CA, since the late 80's. Mostly all commercially available T_1 -based MRI contrast agents are based on Gd^{3+} complexes of DTPA (diethylenetriamine pentaacetic acid) or DOTA (1,4,7,10-Tetraazacyclododecane-1,4,7,10-tetraacetic acid) derivatives. Nevertheless, amongst these, only one is specific: gadofosveset (**Vasovist**[®]; **Alblatar**[®]), used for the targeting of human serum albumin. Figure 1a shows the chemical structure of four Gd^{3+} complexes in clinical use, **Dotarem**[®] (DOTA-based), **Magnevist**[®] (DTPA-based), **ProHance**[®] (HP-DO3A, 2,2',2''-[10-(2-hydroxypropyl)-1,4,7,10-tetraazacyclododecane-1,4,7-triyl]triacetate) and **Vasovist**[®] (DTPA-based).

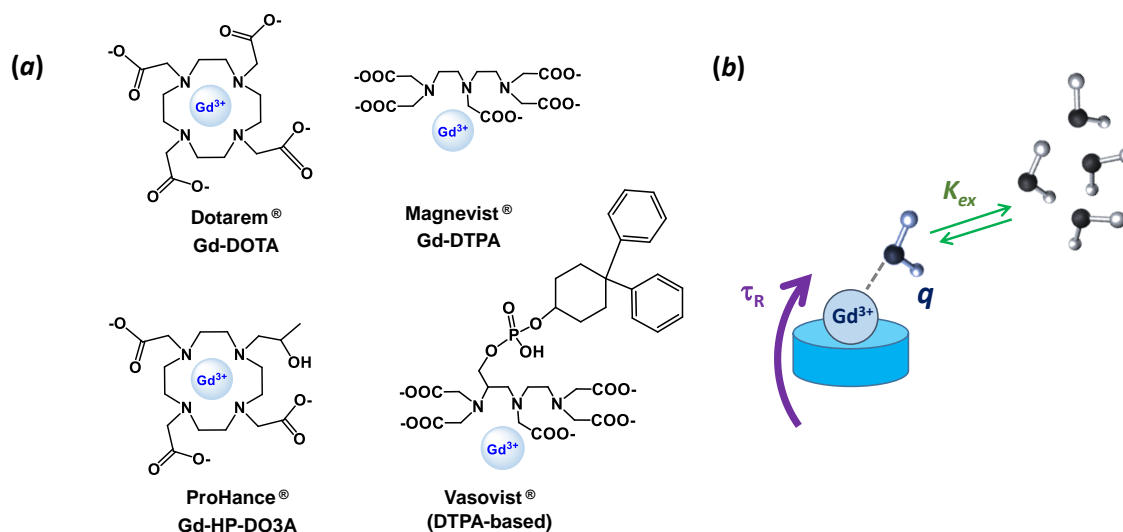


Figure 1. (a) Chemical structure of four Gd³⁺ complexes in clinical use, **Dotarem**[®], **Magnevist**[®], **ProHance**[®] and **Vasovist**[®]; (b) schematic representation of the parameters influencing the relaxivity, that are prone to (chemical) modification: q = number of water molecules directly bound to the Gd³⁺, k_{ex} = water exchange rate and τ_R = rotational correlation time.

Several parameters govern the paramagnetic enhancement efficacy of a CA (or relaxivity, r_1 , expressed per millimolar concentration of Gd³⁺, in $\text{mM}^{-1} \cdot \text{s}^{-1}$) but the main ones that can be tuned easily by the chemists while designing novel and more efficient CAs are: (1) the number of water molecules directly bound to the Gd³⁺ ion, q (hydration number); (2) the water exchange rate of these water molecules with those of the bulk, k_{ex} and (3) the rotational correlation time of the complex, τ_R [1]. A schematic representation of these parameters is depicted in Figure 1b.

The CAs in clinical use are low molecular weight Gd³⁺-based complexes (0.5–1 KDa) with one water molecule in the inner-sphere, which relaxivities range from 3 to 5 $\text{mM}^{-1} \cdot \text{s}^{-1}$ at 1.5 or 3 T (clinical magnetic fields). When administered, these imaging probes will distribute within the organism without a specific target (except for **Vasovist**[®]) and are able to give information on pathologies that result in changes in the vascular volume, perfusion and permeability of the tissues/organs. Such alterations occur typically in more advanced stages of disease. The use of targeted probes that are able to highlight modifications at a molecular/cellular level, before any clinical phenotype of disease is observable, is highly desired.

Even though the design of novel targeted probes is an active research field, the majority of the imaging probes reported in the literature is not in clinical application but still in preclinical validation phase, mostly in phase I or II clinical trials. **Vasovist**[®] has seen its production coming to an end due to insufficient sale numbers, while for example **Gd-ESMA**, an elastin-specific contrast agent, from Lantheus Medical Imaging (see below) is their pipeline in late-stage preclinical studies. There is a clear need for more translational efforts.

Overcoming the low MRI sensitivity

Due to the lack of sensitivity of MRI, relatively high concentrations of CA (mM range) need to be injected to generate local variation in the water signal intensity and, therefore, detectable signal.

Typical biomarkers include receptors or proteins which are overexpressed in case of disease. These are present in vivo usually in low concentrations, often in nM scale. The formation of protein “microdomains” can occur, due to different conformation of a protein and could lead to higher “retention” of a CA and thus to its higher local concentrations. By consequence, a higher local signal enhancement can occur. Estimations based on the parameters of the clinical CA available and the recommended injected dose for an MRI probe (0.1 mmol Gd³⁺/kg), showed that to get a

detectable signal enhancement, a minimum of 100 μM Gd^{3+} local concentration is needed. In case of “microdomain” this detection limit can be up to 2.5-fold lower [2,3].

Signal amplification strategies are then required to achieve good images, enabling the assessment of the desired biomarkers. Among the reported strategies are: accumulation of a large number of Gd^{3+} at the site of interest, by using macromolecular systems (e.g., polymers or nanoparticles); and the use of targeted probes, which have their efficacy changing when binding to their biomarker. The rational design of novel generation of CA is in general accompanied by the optimization of the stability and relaxivity features of the Gd^{3+} complex unit.

2. Rational Design of Targeted Contrast Agents

Different targeting moieties can be used to achieve a specific binding to the chosen biomarker. Figure 2 summarizes the type of moieties potentially used: in general, the probes are based on a chelating unit for the Gd^{3+} (aiming to guarantee a good kinetic inertness and thermodynamic stability of the metal complex but also the presence of at least one water molecule in the inner-sphere), which is conjugated to a small molecule, antibody, protein or peptide via a linker (its length and type can vary, ensuring that the good affinity towards the target is not affected by the presence of the metal complex). When bound to a highly concentrated biomarker in vivo (e.g., human serum albumin), the complex “MRI probe–biomarker” has a higher rotational correlation time, yielding higher relaxivity and hence a higher enhanced signal. If the biomarker is a receptor (lower in vivo concentrations), the signal enhancement results mostly from the high local concentration of the CA (multimeric-like effect).

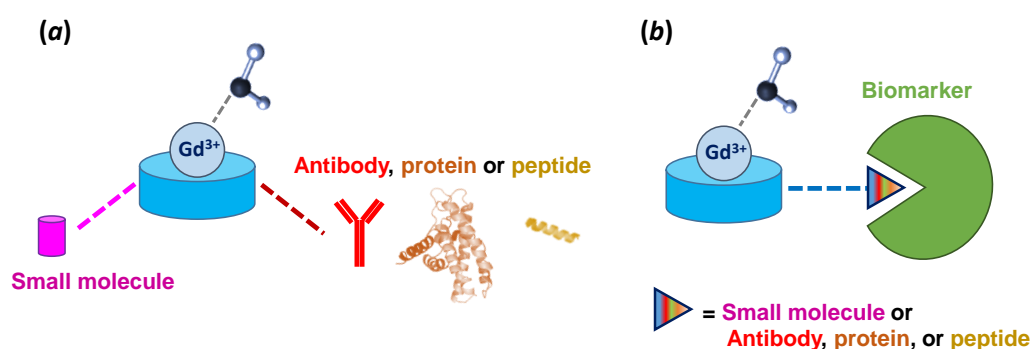


Figure 2. Schematic representation of targeted contrast agents (a) and their interaction with the specific biomarker (b).

Other strategies include the development of macromolecules (usually nanoparticles, the most explored ones being liposomes) that incorporate, within the same unit, a high payload of Gd^{3+} ions and a targeting moiety. Gd^{3+} containing nanoparticle based CA have been revised elsewhere [4–8].

T_2 -weighted based contrast agents for cell tracking or specific targeting have also been developed [9–11].

2.1. Pharmacokinetics, Specificity and Affinity of a Contrast Agent

The biomarkers generally chosen as MRI targets (in general cell surface receptors or extracellular proteins) do not require the contrast agent being able to penetrate the tissue/organ and leave the extravascular compartment. The biodistribution properties of a CA are highly dependent on its size, shape and charge. Small-molecular CA injected intravenously are in general rapidly distributed in the vascular system and eliminated through the kidneys, where particles below 5 nm are filtered regardless of their charge. Larger molecules can undergo adsorption or opsonization by serum proteins and can see their size altered: the in vivo hydrodynamic diameter is typically higher than their in vitro one. This affects their blood clearance and half-life. These larger molecules are eliminated in the kidneys depending on their global charge and size. Macromolecules or particles larger than 8 nm do not

undergo glomerular filtration and are excreted through the hepatobiliary system [12–14]. Such aspects can be considered when conceiving a novel probe, depending on the aimed biodistribution and half-life.

The affinity and specificity towards the target when designing a targeted CA is a major concern. It is desired to achieve a good specificity in order to guarantee that the signal observed is due to the binding towards the protein/tissue of interest. It is also important to have a good reversible affinity, within the time-scale of the imaging protocol. The large majority of the reported targeted-CAs have affinities in the nM to μM range, which seems to be sufficient to perform an MRI, while avoiding the triggering of an immune response from the body, due to the presence of the CA.

2.2. Small Molecules versus Antibody, Protein or Peptide

Compared to their protein-based counterpart probes, small molecule-based and peptide-based probes present a more straightforward chemical and relaxometric characterization and are more easily tuned in terms of improving their *in vivo* stability.

The use of small peptides instead of small molecules to target the same biomarker usually leads to stronger binding affinity and selectivity. Moreover, small peptides are in general promising targeting units when compared with full proteins, mainly due to their appealing properties such as low immunogenicity leading to high biocompatibility, more resistant to *in vivo* enzymatic degradation, favourable pharmacokinetics with fast excretion, good tissue distribution and fast clearance from blood. Peptide structure modifications are often used to adjust their stability and half-life. These include the use of *D*-amino acid residues, cyclization and replacement of peptide bonds with amide bond surrogates.

On the other hand, the use of an antagonist peptide enables better target uptake with comparable binding affinity and no active internalization, compared to agonist peptides. These differences are mostly due to a higher number of binding sites of antagonists and their slower dissociation from the receptor. Antagonist peptides are also more resistant to cell membrane enzymes, which might also contribute to the higher uptake of antagonist peptides [15,16].

3. Different Targets Moieties for the Same Biomarker: Selected Examples

Serum albumin is a highly available plasma protein and has been the biomarker of choice for blood pool contrast agents. Extracellular matrix (ECM) proteins are also vastly explored as biomarkers for several diseases, namely for different types of cancer, metastasis or cardiovascular diseases (CVD) [17,18].

Below are selected examples of MRI targeted probes for serum albumin, ECM proteins (elastin, tropoelastin, collagen, fibrin and fibronectin), epidermal growth factor receptor, protein tyrosine phosphatase mu and amyloid aggregated-like proteins.

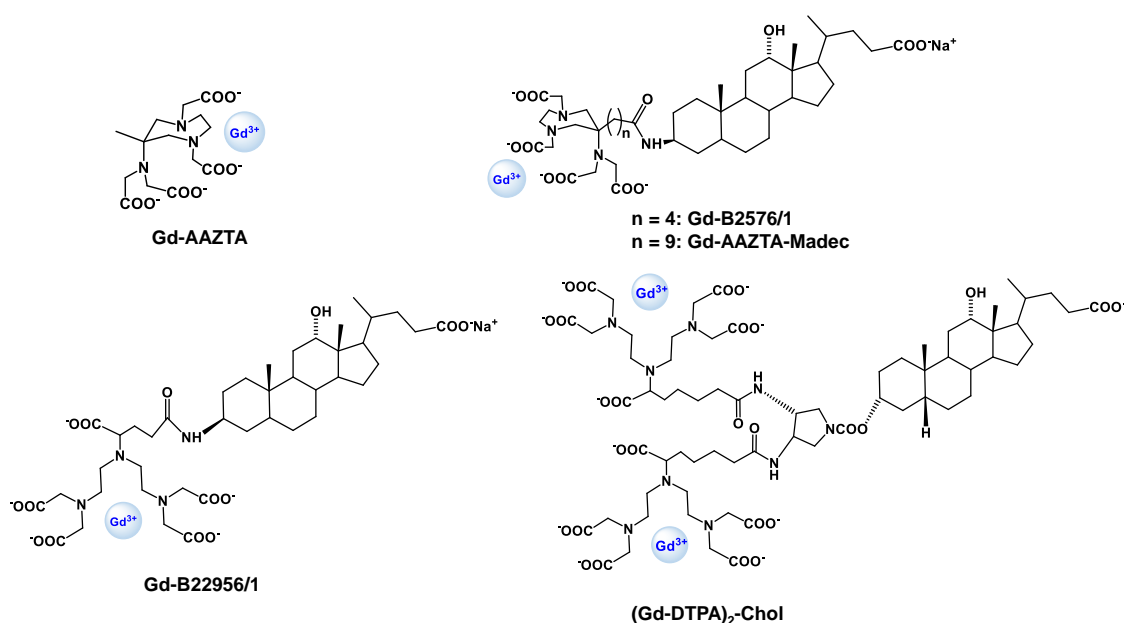
3.1. Human Serum Albumin (HSA)

Human serum albumin (HSA) is the protein present in higher concentration in the blood (≈ 0.6 mM). Several research groups have developed blood pool probes which target HSA, based on different targeting approaches. From the reported probes, **Vasovist**[®] (Figure 1a) has reached clinical application but its production has been discontinued in 2017 due to poor sales.

The structure of **Vasovist**[®] is based on a biphenylcyclohexyl moiety, conjugated to a **Gd-DTPA** unit via a phosphodiester linker, which binds HSA with an affinity of 100 μM . This probe has a relaxivity of $6.6 \text{ mM}^{-1} \cdot \text{s}^{-1}$ in its “free form”, while in the presence of HSA containing human plasma it reaches $42 \text{ mM}^{-1} \cdot \text{s}^{-1}$, at 0.47 T [19,20]. Indeed, the rotational correlation time is the key parameter which accounts for this relaxivity increase: τ_R of **Gd-DTPA** is 58 ps, while for the “complex” **Vasovist-HSA** it is 3000–4000 ps [1].

HSA-probes based on different chelate scaffolds have also been developed. **Gd-AAZTA** (6-amino-6-methylperhydro-1,4-diazepinetetraacetic acid; Scheme 1) complex has two water molecules

in the coordination sphere of Gd^{3+} and displays a relaxivity of $7.1 \text{ mM}^{-1}\cdot\text{s}^{-1}$ (0.47 T, 25 °C) and a τ_R of 74 ps [21].



Scheme 1. Chemical structures of MRI agents designed for HSA targeting.

The use of this scaffold as chelating unit, conjugated to different targeting moieties has led to higher relaxivities of the targeted “free” probes and of their bound form. For example, the AAZTA-based **Gd-B25716/1** [22] and the DTPA chelates **Gd-B22956/1** (in phase I trials) [23,24] and the very recently reported **(Gd-DTPA)₂-Chol** [25], share the same targeting moiety, an analogue of deoxycholic acid (Scheme 1). The use of the AAZTA chelate unit instead of the DTPA brings an extra water molecule to the inner sphere ($q = 2$ for **Gd-AAZTA**), which justifies the higher relaxivity of the complex **Gd-B25716/1** in PBS (at 0.47 T): indeed the r_1 is $13.0 \text{ mM}^{-1}\cdot\text{s}^{-1}$ for **Gd-B25716/1**, 1.5-fold higher when compared with $8.6 \text{ mM}^{-1}\cdot\text{s}^{-1}$ for **B22956/1**. Both AAZTA- and DTPA-based complexes bind to albumin with similar affinities but the relaxivity of the HSA-bound forms is $29.0 \text{ mM}^{-1}\cdot\text{s}^{-1}$ and $26.8 \text{ mM}^{-1}\cdot\text{s}^{-1}$, respectively. In fact, when the AAZTA-based complex binds to HSA the loss of one water molecule from the inner sphere is observed but the expected decrease in relaxivity for the global monohydrated “HSA-(Gd-B25716/1)” complex is somehow compensated by the contribution of second-sphere water molecules present and thus presenting a similar relaxivity than “HSA-(Gd-B22956/1).”

Longo et al. reported on an AAZTA-based CA, **Gd-AAZTA-MADEC** (Scheme 1), conjugated to a deoxycholic acid moiety through a longer spacer, with a 9 CH_2 chain, instead of 2 for **Gd-B25716/1**. The use of a longer linker results in a higher affinity towards HSA ($\approx 1 \mu\text{M}$), about 100-fold higher compared to the aforementioned CA. This improved affinity, together with optimal pharmacokinetic and relaxometric properties (blood half-life of 32.6 min; r_1 of $13.9 \text{ mM}^{-1}\cdot\text{s}^{-1}$ in its “free form” and $38.7 \text{ mM}^{-1}\cdot\text{s}^{-1}$ in the presence of HSA (0.47 T)) make this Gd-based complex a good blood pool CA (Figure 3). **Gd-AAZTA-MADEC** has been tested in vivo, showing significant enhancement of the vasculature and extravasation inside tumour for a prolonged period of time [26].

The recently reported dinuclear Gd^{3+} complex **(Gd-DTPA)₂-Chol** has a relaxivity of $7.7 \text{ mM}^{-1}\cdot\text{s}^{-1}$ in saline and $21.2 \text{ mM}^{-1}\cdot\text{s}^{-1}$ in presence of HSA. The use of a dimer and thus its increase in molecular weight did not lead to a high gain of relaxivity. With similar in vivo “bond” relaxivities for **Gd-B22956/1** and **(Gd-DTPA)₂-Chol** as well as their HSA affinity ($\approx 125 \mu\text{M}$), **(Gd-DTPA)₂-Chol** stands out for its longer blood half-life of 128 min, about 7-fold higher than the half-lives of **Gd-B22956/1** (17.5 min [25]), **Vasovist**[®] (23 min [20]) or **Gd-DTPA** (17.7 min [25]).

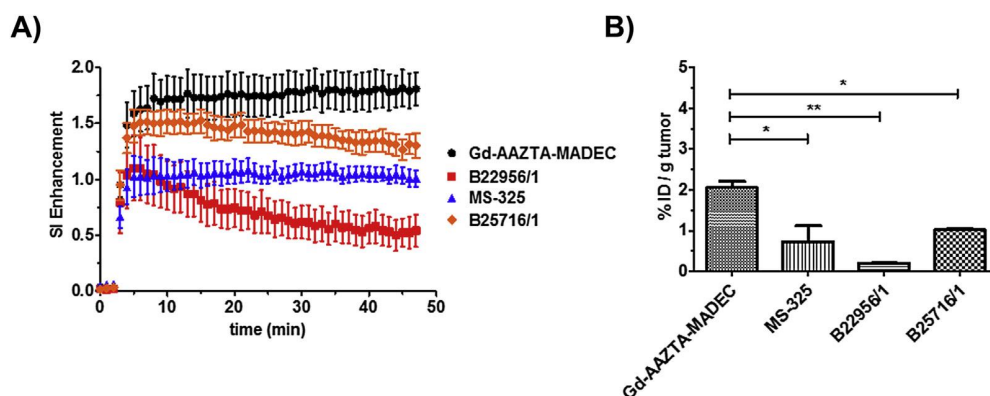
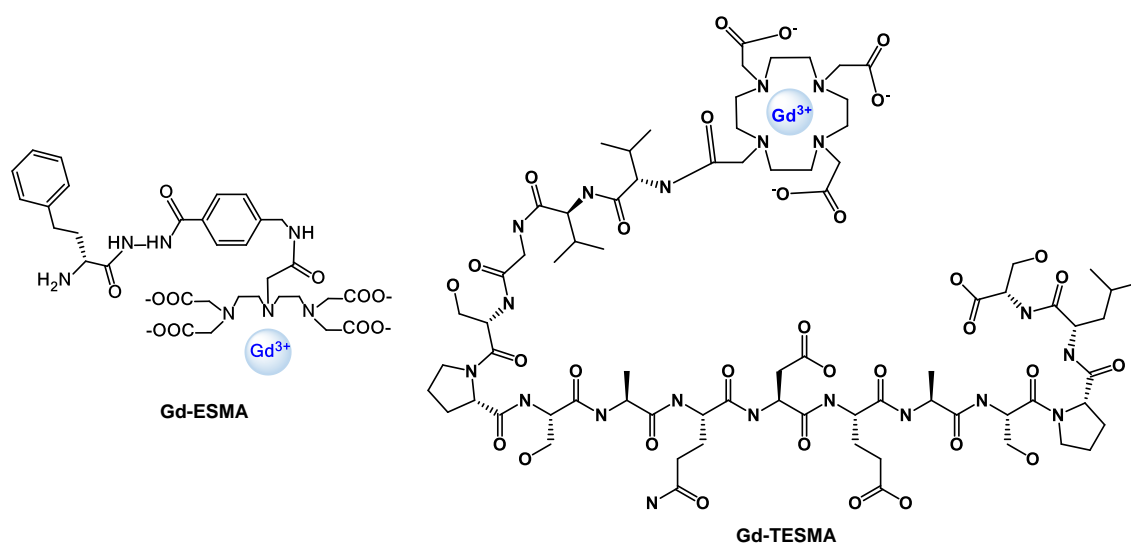


Figure 3. Kinetic study of MRI signal intensity enhancement in tumour of C57BL/6 mice transplanted subcutaneously with B16F10 melanoma cells, with intravenous injection (0.05 mmol Gd^{3+} /kg) of Gd-AAZTA-MADEC (circles), Vasovist® (MS-325) (triangles), Gd-B22956/1 (squares) and Gd-B25716/1 (diamonds) (A) and the Gd^{3+} accumulation within tumour tissue at 60 min post-injection (B). Reprinted with permission from Ref. [26] (Copyright 2016 Elsevier).

3.2. Elastin/Tropoelastin

Elastin is the most abundant protein in the ECM. Dysfunctional ECM contributes to the initiation, progression and complication of arterial diseases, including abdominal aortic aneurysm and atherosclerosis. Elastin in its mature form is an insoluble fibre, consisted of tropoelastin soluble monomers crosslinked by the enzyme Lysil Oxidase (LOX). Tropoelastin is typically produced and converted into elastin in the late fetal and early neonatal periods. Normal arteries contain mature elastin but insignificant amounts of tropoelastin, whose production is resumed in case of disease [17,27].

Elastin has been explored as a biomarker for cardiovascular diseases (CVD) and an MRI contrast agent Gd-ESMA (Scheme 2) was described by Onthank et al., which is now in late-stage preclinical studies led by Lantheus Medical Imaging [28,29]. This CA was validated in animal models of different CVD, such as atherosclerosis [28], aortic abdominal aneurysm [30] and myocardial infarction [31]. Its structure was primarily based on a DTPA chelate, later on developed as a DOTA derivative, conjugated to a single amino acid *D*-phenylalanine. The relaxivity of Gd-ESMA is $4.5 \text{ mM}^{-1} \cdot \text{s}^{-1}$ in its “free” form and $13.7 \text{ mM}^{-1} \cdot \text{s}^{-1}$ when bound to elastin, at 1.5 T [28]. Nevertheless, this compound binds equally to both elastin and tropoelastin (40% binding), with an affinity (K_D) of $1 \pm 0.5 \mu\text{M}$ for elastin and $9.2 \pm 0.7 \mu\text{M}$ for tropoelastin [30].



Scheme 2. Chemical structures of MRI agents designed for elastin and tropoelastin targeting.

Aiming for a better discrimination of elastin and tropoelastin, Phinikaridou et al. have developed a specific CA for tropoelastin. This novel CA consists of a DOTA chelate conjugated to a 15 amino acid peptide: **(Gd-DOTA)-VVGSPSAQDEASPLS** or **Gd-TESMA** (Scheme 2) and allows selective targeting of the monomer (tropoelastin) versus the fibre form (elastin) [32].

The targeting moiety peptide has been selected from the epitope of binding of the elastin-binding protein (EBP) to tropoelastin. EBP is a subunit of the elastin/laminin receptor which is responsible for chaperoning the secreted tropoelastin to the extracellular space.

A good discrimination in the binding to tropoelastin *vs* elastin was achieved with this new probe: $64 \pm 7\%$ versus $1 \pm 2\%$ ($p = 0.001$), respectively, although its affinity remains in the same range as **Gd-ESMA** (K_D of $2.37 \pm 0.05 \mu\text{M}$ for tropoelastin and of $14 \pm 5 \mu\text{M}$ for elastin). This new CA has a high in vitro relaxivity in solution ($11.7 \pm 0.6 \text{ mM}^{-1} \cdot \text{s}^{-1}$) and presents a relaxivity of $44 \pm 1 \text{ mM}^{-1} \cdot \text{s}^{-1}$ when bound to tropoelastin in vitro (0.47 T). In vivo studies on a murine model of atherosclerosis revealed a lower in vivo relaxivity value which drops to $7.15 \text{ mM}^{-1} \cdot \text{s}^{-1}$ (3 T). This difference was attributed to the different (higher) magnetic field and to the fact that some of the binding sites of tropoelastin might be masked in vivo, together with the less accessibility of water within the atherosclerotic lesion.

For this system, the use of a small peptide instead of a single amino acid provided a good in vitro and in vivo discrimination of the monomer versus the fibre and therefore enabling discrimination of diseased and “normal” vessel wall. Figure 4 shows the in vivo MRI comparison of vessel wall enhancement using the elastin (**Gd-ESMA**, 0.2 mmol Gd^{3+}/kg) and tropoelastin (**Gd-TESMA**, 0.2 mmol Gd^{3+}/kg) CAs in control and diseased mice (atherosclerotic apolipoprotein E-deficient murine model ($\text{ApoE}^{-/-}$)). The figure displays the fused maximum intensity projection reconstructed magnetic resonance angiography and delayed-enhanced-MRI after administration of both CA to the same animal scanned 24 h apart, showing focal uptake in the brachiocephalic artery (BCA). The MRI of the BCA acquired from a control animal showed vessel wall uptake of **Gd-ESMA** (panels Figure 4A,B) but no uptake of **Gd-TESMA** (panels Figure 4C,D) due to the lack of tropoelastin in the absence of disease. Nevertheless, MRI of the BCA acquired from a diseased animal showed enhancement of the vessel wall after administration of both agents because of the presence of both cross-linked elastin and tropoelastin in the atherosclerotic lesion. The discrimination of normal versus diseased BCAs is clearer when using **Gd-TESMA**.

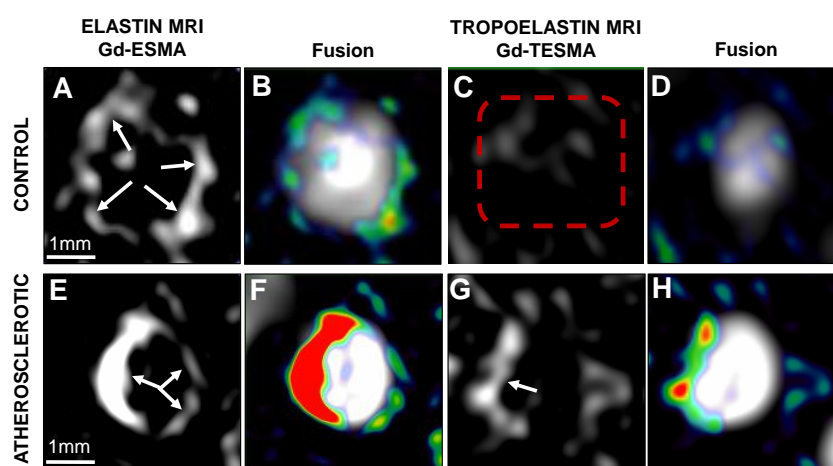
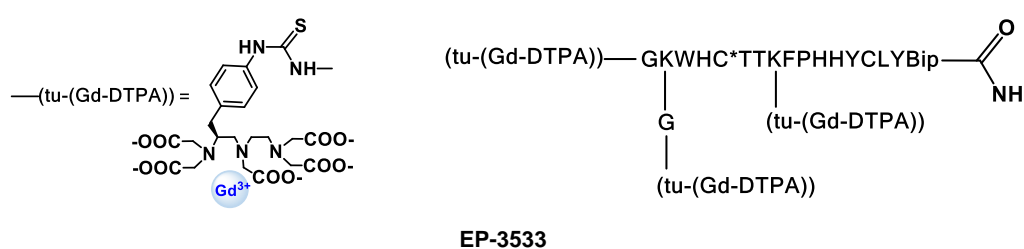


Figure 4. In vivo MRI comparison of vessel wall enhancement using the elastin (**Gd-ESMA**) and tropoelastin (**Gd-TESMA**) in mice (both 0.2 mmol Gd^{3+}/kg): fused maximum intensity projection reconstructed MR angiography and delayed-enhanced-MRI after administration of **Gd-ESMA** and **Gd-TESMA** in the brachiocephalic artery (BCA) of an atherosclerotic $\text{ApoE}^{-/-}$ mouse. (A–D): MRI of the BCA acquired from a control animal, scanned 24 h apart. (E–H): MRI of the BCA acquired from a diseased animal. This figure is adapted with permission of American Heart Association from ref. [32].

3.3. Collagen

There are 28 different types of collagen, mostly present at the ECM as triple-stranded fibres, which can further interact to form networks. They confer tensile strength, regulate cell adhesion, promote cell migration and are also involved in chemotaxis. Imbalance of collagen expression or ratio between types of collagen are associated with several diseases, including CDV and cancer, making them potential disease biomarkers [18].

Several imaging probes have been explored, for example, based on phage display and amino acid mutation studies Caravan et al. were able to identify a collagen binding peptide: GKWHCTTKFPHHYCLY [33]. This peptide has then been conjugated to three Gd-DTPA units and termed **EP-3533** (Scheme 3). This probe has good affinity for type I collagen ($K_D = 1.8 \pm 1.0 \mu\text{M}$) and a relaxivity of $16.1 \text{ mM}^{-1} \cdot \text{s}^{-1}$ per Gd^{3+} (or $48.3 \text{ mM}^{-1} \cdot \text{s}^{-1}$ per molecule) at 1.4 T and has enabled visualization of fibrotic scar versus viable myocardium and blood in a mouse model of chronic infarction [34].



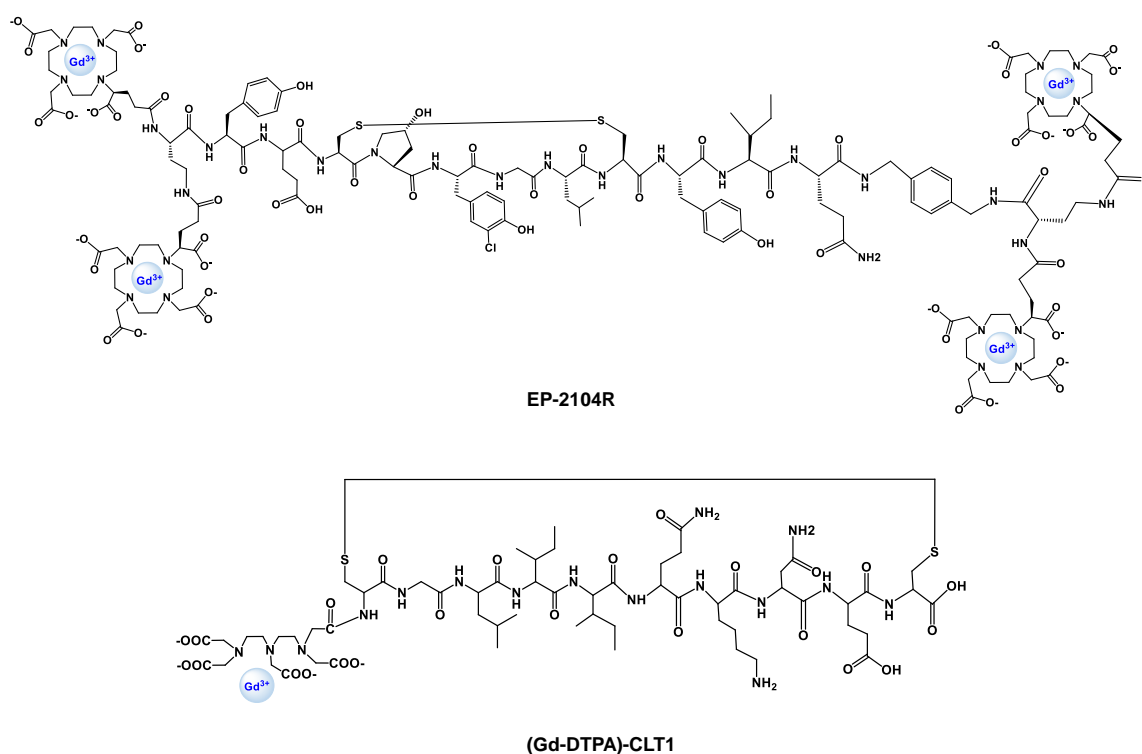
Scheme 3. Structure of EP-3533.

3.4. Fibrin and Fibronectin

Fibrin is the major component of the blood clot. It is involved in wound healing and tissue repair and is implicated in processes of adhesion, proliferation and migration of cells involved in the repairing process. Changes in fibrin expression, or its degradation and organization were associated with a number of pathologies, including thrombosis, infection, inflammation, fibrosis and cancer. Fibronectin is a glycoprotein which contains two major fibrin-binding sites and is enzymatically converted in fibrin. It mediates a large variety of cellular interactions with the ECM and plays an important role in cell adhesion, migration, growth and differentiation [17,18].

3.4.1. Fibrin

Fibrin has been largely explored as imaging target. Amongst the specific contrast agents developed, the majority is based on small peptide moieties. For example, Caravan et al. developed several CAs based on small peptides anchored on DTPA or DOTA chelates and bearing one to four units per molecule, namely, **EP-1873** (DTPA-based) [35] and **EP-2104R** (DOTA-GA-based; Scheme 4) [36] probes containing the peptide ($X_n\text{CPYGLCX}_m$). The chosen peptides bind to fibrin with K_D in the range 4 to 9 μM and have a remarkable selectivity for fibrin over fibronectin (100-fold). Both complexes have 4 Gd^{3+} units and present relaxivities of $84 \text{ mM}^{-1} \cdot \text{s}^{-1}$ ($21 \text{ mM}^{-1} \cdot \text{s}^{-1}$ per Gd^{3+}) and $71.4 \text{ mM}^{-1} \cdot \text{s}^{-1}$ ($17.4 \text{ mM}^{-1} \cdot \text{s}^{-1}$ per Gd^{3+}) at 1.4 T, respectively, when bound to fibrin.



Scheme 4. Structures of EP-2104R and (Gd-DTPA)-CLT1.

EP-2104R allowed detection of thrombus in a rat ischemic stroke model. Figure 5 shows a coronal slice from middle cerebral artery 3D T1-weighted images of the detection of an intracranial thrombus using **EP-2104R**. This probe has reached phase II trials and enabled visualization of 52 patients with previously diagnosed with thrombi in the venous, heart or arterial system [37,38].

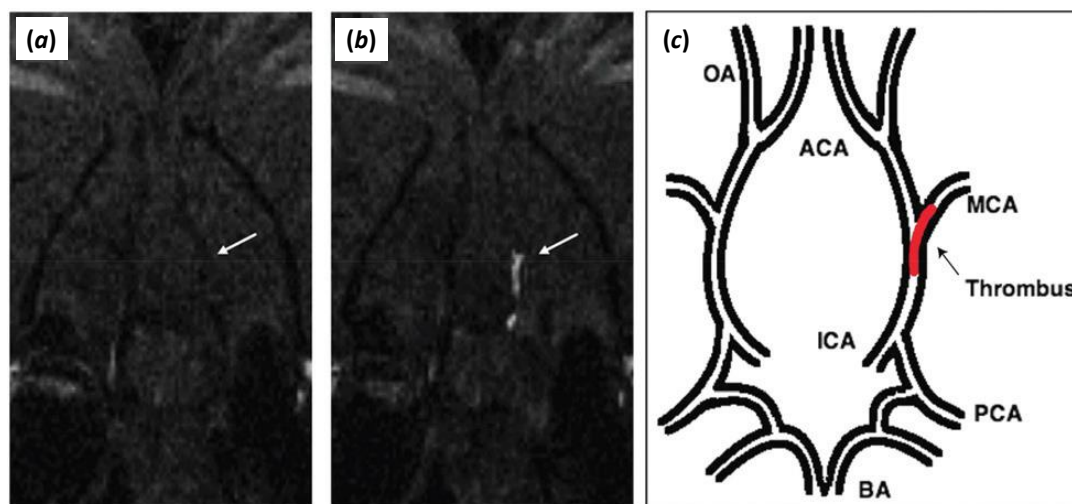
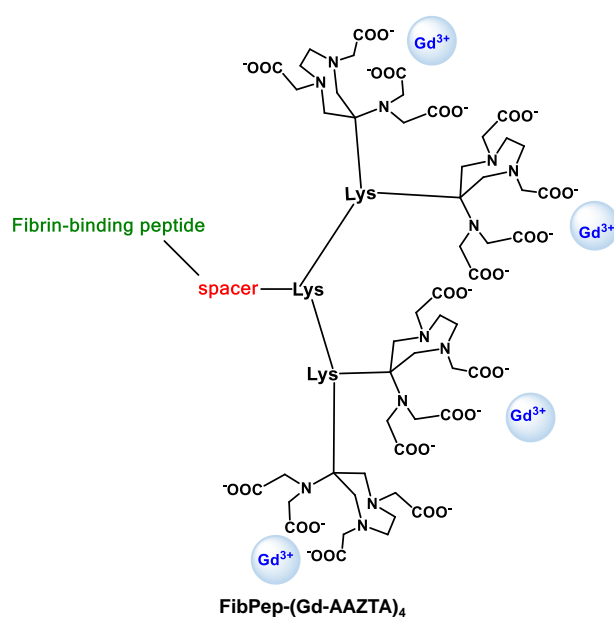


Figure 5. Coronal slice from middle cerebral artery 3D T1-weighted MR images of the detection of an intracranial thrombus (white arrow) in a rat ischemic stroke model using **EP-2104R**: (a) pre-contrast image; (b) post-contrast after injection of **EP-2104R** with clear detection of the thrombus (arrow) located in branch of the internal carotid artery (ICA) with the MCA; (c) schematic representation of the thrombus within the cerebral arterial tree, where BA = basilar artery, PCA = posterior cerebral artery, ICA = internal carotid artery, OA = olfactory artery and ACA = anterior cerebral artery. Reproduced with permission of The Royal Society of Chemistry from Ref. [37] (Copyright 2017 RCS).

Earlier, Lu et al. have explored the cyclic CLT1 peptide (CGLIIQKNEC) conjugated to a DTPA unit (**Gd-DTPA**)-CLT1, Scheme 4), which binds specifically to the complex fibrin-fibronectin. This CA presents a relaxivity of $4.2 \text{ mM}^{-1}\cdot\text{s}^{-1}$ at 3 T and was evaluated in athymic nu/nu mice bearing HT-29 human colon carcinoma xenografts. A good enhancement was observed in the tumour. Due to the involvement of fibrin-fibronectin complexes in several pathologies, the authors claim that (**Gd-DTPA**)-CLT1 has a great potential for cancer detection, as well as diagnosis, characterization of tumour angiogenesis and imaging of wounds and atherosclerosis [39].

Aime et al. followed a similar approach to that of Caravan and co-workers, developing an AAZTA-tetramer conjugated to the same fibrin-binding peptide used for **EP-2104R** ($X_n\text{CPYGLCX}_m$) [40]. This novel probe—**FibPep**-(**Gd-AAZTA**)₄ (Scheme 5)—relies on four Gd-AAZTA(CH₂)₄COOH units, which are coupled to a trilycine scaffold, functionalized with a maleimide function, which is then conjugated to the cyclic 11-amino acid fibrin-binding peptide (FibPep), previously reported by Caravan et al. [36].



Scheme 5. Structure of the tetramer **FibPep-(Gd-AAZTA)₄**.

This novel probe has a relaxivity of $18.5 \pm 0.3 \text{ mM}^{-1}\cdot\text{s}^{-1}$ per Gd^{3+} or $74 \pm 1 \text{ mM}^{-1}\cdot\text{s}^{-1}$ per molecule in water; of $22.5 \pm 0.2 \text{ mM}^{-1}\cdot\text{s}^{-1}$ per Gd^{3+} in serum and higher relaxivity of $58 \pm 13 \text{ mM}^{-1}\cdot\text{s}^{-1}$ per Gd^{3+} in presence of fibrin plasma clots (0.5 T). The binding profile of this CA to fibrin shows specific and unspecific binding regions depending on the concentration range. An affinity (K_D) of $3.0 \pm 0.6 \mu\text{M}$ has been determined by fitting the data for the higher affinity site (up to $10 \mu\text{M}$) [40].

3.4.2. Extradomain B Fibronectin

Prostate cancer still accounts for 30% death of patients, making earlier and more accurate detection of the disease an unmet clinical need. Lu and co-workers have explored four novel MRI contrast agents that target extradomain-B fibronectin (EDB-FN; overexpressed in the ECM of aggressive tumours but absent in healthy tissue), as cancer biomarkers [41–43]. These recent probes are based on HP-DO3A (Figure 1a) or DOTA derivatives conjugated to small peptides which target EDB-FN, via a short PEG linker. The peptides have been identified by phage display and show strong affinity towards human EDB-FN. The first peptide studied is a 7 amino acid residue named ZD2 (TVRTSAD) and has been conjugated to both HP-DO3A [43] and DOTA [42] chelates. **ZD2-(Gd(HP-DO3A))** (K_D of $1.7 \mu\text{M}$)

has a relaxivity of $5.4 \text{ mM}^{-1} \cdot \text{s}^{-1}$ while the one of the analogue **ZD2-(Gd-DOTA)** is $4.1 \text{ mM}^{-1} \cdot \text{s}^{-1}$ at 1.5 T [43].

Another three sequences were also identified and have been conjugated to DOTA derivative, via reaction with *p*-NCS-Bz-DOTA-GA (2,2',2''-(10-(1-carboxy-4-((4-isothiocyanatobenzyl)amino)-4-oxobutyl)-1,4,7,10-tetraazacyclododecane-1,4,7-triyl)triacetic acid) which results in an additional isothiocyanate group in the linker: **GVK-(Gd-DOTA)**, GVK = GVKSYNE; **IGK-(Gd-DOTA)**, IGK = IGKTNTL and **SGV-(Gd-DOTA)**, SGV = SGVKSFA [41].

In silico simulations with the peptides showed their binding patterns towards the EDB-FN (Figure 6), revealing that these peptides bind to different sites of the EDB fragment.

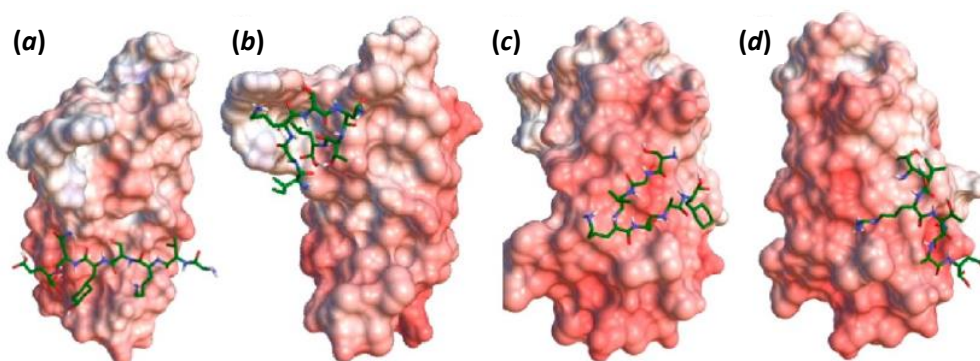


Figure 6. Electrostatic surface of extradomain-B fibronectin fragment (EDB) and 3D stick molecular models (C = green, N = blue, O = red and H = white) of peptides (a) GVK, (b) IGK, (c) SGV and (d) ZD2 fitted to the protein. For the surface of EDB, blue indicates positive charged residues, red represents negative areas and white are neutral regions. Reprinted with permission from Ref. [41] (Copyright, 2017, American Chemical Society).

All compounds have been tested in vivo by MRI in PC3 tumour bearing mice, showing tumour uptake and good signal enhancement compared with the non-specific counterparts Gd-DOTA or Gd-(HP-DO3A). The tumour affinity and specificity were confirmed by studying the in vivo and ex vivo fluorescence of the Cy5.5-peptide derivatives. These additional three probes have similar relaxivities at 1.5 T (4.3 to $4.7 \text{ mM}^{-1} \cdot \text{s}^{-1}$) but the biodistribution studies revealed a stronger binding for IGK peptide that is similar to ZD2.

3.5. Epidermal Growth Factor Receptor/HER2 (EGFR/HER2)

The HER2 epidermal growth factor receptors (EGFR/HER2) are overexpressed in various types of cancer cells and constitute a known biomarker for cancer prognosis. These are already in clinical use as biomarkers, namely for breast cancer but their quantification relies on invasive methods such as biopsy followed by measurement of the proteins by molecular biology techniques and in general lead to inaccurate results. Non-invasive detection of the higher levels of these proteins directly in vivo would simplify the detection and allow treatment monitoring of early stage breast cancer tumours.

Yang et al. have reported on the development of novel type of Gd^{3+} -binding protein MRI probes, ProCA [3,44,45]. The scaffold of these CAs is based on the domain 1 of CD2. This protein is expressed at the surface of natural killer cells and T cells and is implicated in signal transduction and cell adhesion. Its attractive features as scaffold include the rigidity, resistance to pH changes and enzyme cleavage and high tolerance for mutations.

The stable coordination of Gd^{3+} is assured by the presence of five Aspartic acid (Asp or D) and Glutamic acid (Glu or E) carboxylic side chains or by incorporating unnatural amino acids into the sequence, whose coordination sphere is completed by two water molecules. The binding pocket design takes into account the good exposition of Gd^{3+} towards the bulk water, enabling an exchange to happen, essential for MRI. This coordination design has been optimized by computer simulations

(Figure 7) and enabled the design of different CA's. The first generation, ProCA1, has a relaxivity of $117 \text{ mM}^{-1}\cdot\text{s}^{-1}$ at 1.5 T and $48 \text{ mM}^{-1}\cdot\text{s}^{-1}$ at 3 T (medical fields) and a q of 2. The thermodynamic stability of these complexes is relatively low ($\log K_{\text{ML}} \approx 12.1$ [44]; while $\log K_{\text{ML}}(\text{Gd-DTPA}) \approx 22.46$ [1]) but improved stability has been achieved for the latest generation ProCA3, displaying a $\log K_{\text{ML}}$ of 21.6 [46]. Nonetheless, this first generation showed good stability (no transmetallation) when tested under conditions simulating the extracellular environment and no effect of other biological metal ions on the relaxivities of ProCAs was observed [46]. Further improvement of this generation of CA included its PEGylation for a better blood half-life, which also resulted in an increase of 30–100% in their relaxivity.

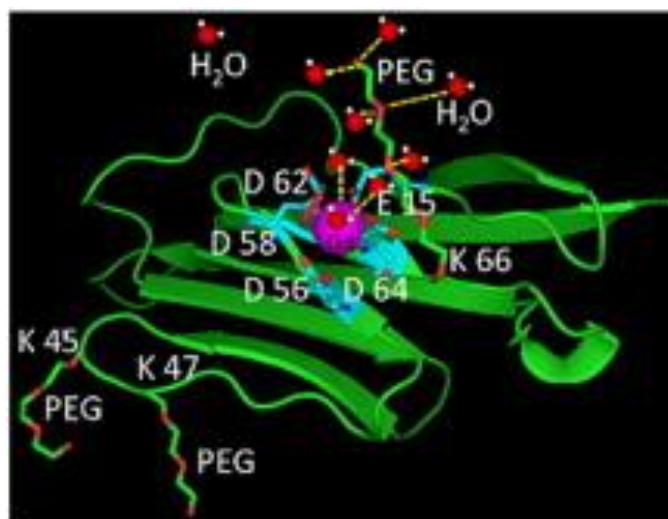


Figure 7. Modelled structure of the coordination of Gd^{3+} (purple) in ProCA1 with PEG chain (red), including outer sphere water molecules associated. (D = aspartic acid; E = glutamic acid and K = lysine) Reprinted with permission from Ref. [44] (copyright, 2012, Elsevier).

Moreover, specific ProCA-based CAs targeting HER2 (ProCA1.affi). The targeted CAs consist on the conjugation of ProCA1 to a targeted moiety using antibodies or affibodies, either by conjugation via a flexible linker to the C-terminus of the Gd^{3+} -binding protein or by a biotin-avidin method [3,45]. The successful targeting has been validated in vivo in nude mice xenograft models of SKOV3 and MDA-MB-231 human cell lines for HER2. Structure improvements allowed the use of 60- to 100-fold lower dose injections when compared to the clinical doses [3,44,45].

The same authors also reported on other ProCA1-based targeting probes, for example ProCA1.GRPC was proposed as gastrin-releasing peptide receptor probe and tested in PC-3 tumour xenograft mice [3,46].

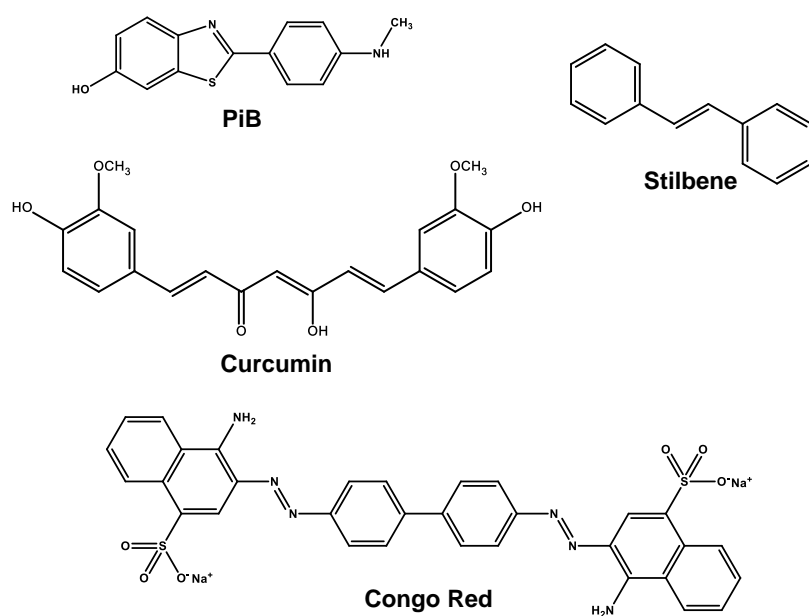
3.6. Protein Tyrosine Phosphatase Mu ($\text{PTP}\mu$)

Glioblastoma multiforme (GBM) is a highly lethal brain tumour characterized by its fast proliferation and ability to spread. Normal brain astrocytomas express the receptor protein tyrosine phosphatase mu ($\text{PTP}\mu$) in normal conditions, while GBM downregulates the full length expression of this protein. One of the resulting fragments remains associated with GBM tissue setting an interesting biomarker for these tumours. Brady-Kalmay and co-workers have studied MRI probes that target $\text{PTP}\mu$ based on four peptides SBK1-4, designed from the epitopes of interaction of $\text{PTP}\mu$ with cell adhesion molecules of μ (SBK1 and 2) or immunoglobulin (SBK3 and 4) domains. From these, SBK2 and SBK4 showed to bind better to $\text{PTP}\mu$ [47] and the same group reported on the development of an MRI probe based on the peptide SBK2 (GEGDDFNWEQVNTLTKPTSD) conjugated to 3 Gd-DOTA units via a tris-propargyl linker, **SBK2-Tris-(Gd-DOTA)₃** [48]. This probe has a relaxivity of $8.3 \text{ mM}^{-1}\cdot\text{s}^{-1}$ per

Gd³⁺ at 1.41 T and is able to target heterotopic xenograft model of brain tumour, showing prolonged tumour retention when compared with a non-specific CA and a SBK2-scrambled-(Gd-DOTA)₃ version. More recently, a single Gd³⁺ unit version of this CA, using a lysine residue as spacer, **SBK2-Lys-(Gd-DOTA)**, showed a relaxivity of $8.4 \pm 0.1 \text{ mM}^{-1} \cdot \text{s}^{-1}$ at 1.41 T ($6.0 \pm 0.1 \text{ mM}^{-1} \cdot \text{s}^{-1}$ at 9.4 T) allowing a good tumour enhancement, in both heterotopic and orthotopic glioma murine models [49]. Importantly, this recent “mono-Gd³⁺” version could be injected in the typical dose (0.1 mmol Gd³⁺/kg), while the tris-DOTA version could only be detected using 0.2 mmol Gd³⁺/kg.

3.7. Misfolded Amyloid Aggregated-Like Proteins

Aggregation of misfolded proteins is a common hallmark of highly debilitating diseases such as amyotrophic lateral sclerosis, type II diabetes and Parkinson’s and Alzheimer’s diseases. The development of novel non-invasive probes which target misfolded proteins at the origin of these diseases, such as superoxide dismutase, human amylin, α -Synuclein, hyperphosphorylated tau protein and in particular Amyloid- β for Alzheimer’s disease, have been widely explored and reviewed [50]. The majority of the probes is based on Gd³⁺-complexes linked to small molecules, peptides or antibodies. Small molecule-based CAs are mostly based on derivatives of: (1) Pittsburgh compound B (PiB), a derivative of the thioflavin T which binds to fibrillar A β amyloid deposits in situ; (2) Curcumin; (3) Congo Red and (4) stilbene. All structures are depicted in Scheme 6.



Scheme 6. Structures of small molecule derivatives for A β targeting: Pittsburgh compound B (PiB), curcumin, stilbene and Congo Red.

Geraldes, Tóth and co-workers explored a series of DOTA-based complexes bearing a modified PiB unit conjugated via different linkers (different length and chemical nature, leading to different charge and lipophilicity of the probes; Scheme 7) [51]. These CAs have relaxivities of $\approx 6 \text{ mM}^{-1} \cdot \text{s}^{-1}$ in water and $\approx 14 \text{ mM}^{-1} \cdot \text{s}^{-1}$ in the presence of aggregated A β protein (0.47 T) and showed affinities towards A β _{1–40} within the 70–200 μM range.

Importantly, radiolabelled analogues (¹¹¹In [52], ⁶⁸Ga [53]) of the probes showed promising brain uptake in vivo, both in wild-type and Alzheimer’s disease mice models.

Indeed, the biggest challenge of the probes developed so far relies on the difficulty of blood-brain barrier crossing by the final complexes.

3. Xue, S.; Qiao, J.; Pu, F.; Cameron, M.; Yang, J.J. Design of a novel class of protein-based magnetic resonance imaging contrast agents for the molecular imaging of cancer biomarkers. *WIREs Nanomed. Nanobiotechnol.* **2013**, *5*, 163–179. [[CrossRef](#)] [[PubMed](#)]
4. Zhang, P.; Cui, Y.; Anderson, C.F.; Zhang, C.; Li, Y.; Wang, R.; Cui, H. Peptide-based nanoprobe for molecular imaging and disease diagnostics. *Chem. Soc. Rev.* **2018**, *47*, 3490–3529. [[CrossRef](#)] [[PubMed](#)]
5. Zhao, Y.; Peng, J.; Li, J.; Huang, L.; Yang, J.; Huang, K.; Li, H.; Jiang, N.; Zheng, S.; Zhang, X.; et al. Tumor-Targeted and Clearable Human Protein-Based MRI Nanoprobes. *Nano Lett.* **2017**, *17*, 4096–4100. [[CrossRef](#)]
6. Zhou, Z.; Han, Z.; Lu, Z.-R. A targeted nanoglobular contrast agent from host-guest self-assembly for MR cancer molecular imaging. *Biomaterials* **2016**, *85*, 168–179. [[CrossRef](#)]
7. Vithanarachchi, S.M.; Allen, M.J. Strategies for Target-Specific Contrast Agents for Magnetic Resonance Imaging. *Curr. Mol. Imaging* **2012**, *1*, 12–25. [[CrossRef](#)] [[PubMed](#)]
8. Sanders, H.M.H.F.; Strijkers, G.J.; Mulder, W.J.M.; Huinink, H.P.; Erich, S.J.F.; Adan, O.C.G.; Sommerdijk, N.A.J.M.; Merckx, M.; Nicolay, K. Morphology, binding behavior and MR-properties of paramagnetic collagen-binding liposomes. *Contrast Media Mol. Imaging* **2009**, *4*, 81–88. [[CrossRef](#)]
9. Ding, C.; Wu, K.; Wang, W.; Guan, Z.; Wang, L.; Wang, X.; Wang, R.; Liu, L.; Fan, J. Synthesis of a cell penetrating peptide modified superparamagnetic iron oxide and MRI detection of bladder cancer. *Oncotarget* **2017**, *8*, 4718–4729. [[CrossRef](#)]
10. Gu, L.; Li, X.; Jiang, J.; Guo, G.; Wu, H.; Wu, M.; Zhu, H. Stem cell tracking using effective self-assembled peptide-modified superparamagnetic nanoparticles. *Nanoscale* **2018**, *10*, 15967–15979. [[CrossRef](#)]
11. Ahrens, E.T.; Bulte, J.W.M. Tracking immune cells in vivo using magnetic resonance imaging. *Nat. Rev. Immunol.* **2013**, *13*, 755–763. [[CrossRef](#)]
12. Jaspers, K.; Aerts, H.J.W.L.; Leiner, T.; Oostendorp, M.; van Riel, N.A.W.; Post, M.J.; Backes, W.H. Reliability of pharmacokinetic parameters: Small vs. medium-sized contrast agents. *Magn. Reson. Med.* **2009**, *62*, 779–787. [[CrossRef](#)] [[PubMed](#)]
13. Longmire, M.; Choyke, P.L.; Kobayashi, H. Clearance properties of nano-sized particles and molecules as imaging agents: Considerations and caveats. *Nanomedicine* **2008**, *3*, 703–717. [[CrossRef](#)]
14. Strijkers, G.J.; Mulder, W.J.; van Tilborg, G.A.; Nicolay, K. MRI contrast agents: Current status and future perspectives. *Anticancer Agents Med. Chem.* **2007**, *7*, 291–305. [[CrossRef](#)] [[PubMed](#)]
15. Ruzza, P.; Calderan, A. Radiolabeled peptide-receptor ligands in tumor imaging. *Expert Opin. Med. Diagn.* **2011**, *5*, 411–424. [[CrossRef](#)]
16. Sun, X.; Li, Y.; Liu, T.; Li, Z.; Zhang, X.; Chen, X. Peptide-based imaging agents for cancer detection. *Adv. Drug Deliv. Rev.* **2017**, *110–111*, 38–51. [[CrossRef](#)]
17. Frantz, C.; Stewart, K.M.; Weaver, V.M. The extracellular matrix at a glance. *J. Cell Sci.* **2010**, *123*, 4195–4200. [[CrossRef](#)] [[PubMed](#)]
18. Nyström, A.; Bruckner-Tuderman, L. Matrix molecules and skin biology. *Semin. Cell Dev. Biol.* **2018**. [[CrossRef](#)]
19. Lauffer, R.B.; Parmelee, D.J.; Dunham, S.U.; Ouellet, H.S.; Dolan, R.P.; Witte, S.; McMurry, T.J.; Walovitch, R.C. MS-325: Albumin-targeted contrast agent for MR angiography. *Radiology* **1998**, *207*, 529–538. [[CrossRef](#)]
20. Parmelee, D.J.; Walovitch, R.C.; Ouellet, H.S.; Lauffer, R.B. Preclinical evaluation of the pharmacokinetics, biodistribution, and elimination of MS-325, a blood pool agent for magnetic resonance imaging. *Investig. Radiol.* **1997**, *32*, 741–747. [[CrossRef](#)]
21. Aime, S.; Calabi, L.; Cavallotti, C.; Gianolio, E.; Giovenzana, G.B.; Losi, P.; Maiocchi, A.; Palmisano, G.; Sisti, M. [Gd-AAZTA]-: A New Structural Entry for an Improved Generation of MRI Contrast Agents. *Inorg. Chem.* **2004**, *43*, 7588–7590. [[CrossRef](#)]
22. Gianolio, E.; Cabella, C.; Colombo Serra, S.; Valbusa, G.; Arena, F.; Maiocchi, A.; Miragoli, L.; Tedoldi, F.; Uggeri, F.; Visigalli, M.; et al. B25716/1: A novel albumin-binding Gd-AAZTA MRI contrast agent with improved properties in tumor imaging. *J. Biol. Inorg. Chem.* **2014**, *19*, 715–726. [[CrossRef](#)] [[PubMed](#)]
23. Cavagna, F.M.; Lorusso, V.; Anelli, P.L.; Maggioni, F.; de Haën, C. Preclinical Profile and Clinical Potential of Gadocoletic Acid Trisodium Salt (B22956/1), a New Intravascular Contrast Medium for MRI. *Acad. Radiol.* **2002**, *9*, S491–S494. [[CrossRef](#)]

24. Noce, A.L.; Stoelben, S.; Scheffler, K.; Hennig, J.; Lenz, H.M.; Ferla, R.L.; Lorusso, V.; Maggioni, F.; Cavagna, F. B22956/1, a New Intravascular Contrast Agent for MRI: First Administration to Humans—Preliminary Results. *Acad. Radiol.* **2002**, *9*, S404–S406. [[CrossRef](#)]
25. La Cava, F.; FringuelloMingo, A.; Miragoli, L.; Terreno, E.; Cappelletti, E.; Lattuada, L.; Poggi, L.; Colombo Serra, S. Synthesis, Characterization, and Biodistribution of a Dinuclear Gadolinium Complex with Improved Properties as a Blood Pool MRI Agent. *ChemMedChem* **2018**, *13*, 824–834. [[CrossRef](#)] [[PubMed](#)]
26. Longo, D.L.; Arena, F.; Consolino, L.; Minazzi, P.; Geninatti-Crich, S.; Giovenzana, G.B.; Aime, S. Gd-AAZTA-MADEC, an improved blood pool agent for DCE-MRI studies on mice on 1 T scanners. *Biomaterials* **2016**, *75*, 47–57. [[CrossRef](#)]
27. Brooke, B.S.; Bayes-Genis, A.; Li, D.Y. New insights into elastin and vascular disease. *Trends Cardiovasc. Med.* **2003**, *13*, 176–181. [[CrossRef](#)]
28. Makowski, M.R.; Wiethoff, A.J.; Blume, U.; Cuello, F.; Warley, A.; Jansen, C.H.; Nagel, E.; Razavi, R.; Onthank, D.C.; Cesati, R.R.; et al. Assessment of atherosclerotic plaque burden with an elastin-specific magnetic resonance contrast agent. *Nat. Med.* **2011**, *17*, 383–388. [[CrossRef](#)]
29. Onthank, D.; Yalamanchili, P.; Cesati, R.; Lazewatsky, J.; Azure, M.; Hayes, M.; Kavosi, M.; Spencer, K.; Sousa, D.; Wexler, E.; et al. Abstract 1914: BMS753951: A Novel Low Molecular Weight Magnetic Resonance Contrast Agent Selective for Arterial Wall Imaging. *Circulation* **2007**, *116*, 411–412.
30. Botnar, R.M.; Wiethoff, A.J.; Ebersberger, U.; Lacerda, S.; Blume, U.; Warley, A.; Jansen, C.H.; Onthank, D.C.; Cesati, R.R.; Razavi, R.; et al. In vivo assessment of aortic aneurysm wall integrity using elastin-specific molecular magnetic resonance imaging. *Circ. Cardiovasc. Imaging* **2014**, *7*, 679–689. [[CrossRef](#)]
31. Protti, A.; Lavin, B.; Dong, X.; Lorrio, S.; Robinson, S.; Onthank, D.; Shah, A.M.; Botnar, R.M. Assessment of Myocardial Remodeling Using an Elastin/Tropoelastin Specific Agent with High Field Magnetic Resonance Imaging (MRI). *J. Am. Heart Assoc.* **2015**, *4*, e001851. [[CrossRef](#)]
32. Phinikaridou, A.; Lacerda, S.; Lavin, B.; Andia, M.E.; Smith, A.; Saha, P.; Botnar, R.M. Tropoelastin: A novel marker for plaque progression and instability. *Circ. Cardiovasc. Imaging* **2018**, *11*, e007303. [[CrossRef](#)] [[PubMed](#)]
33. Caravan, P.; Das, B.; Deng, Q.; Dumas, S.; Jacques, V.; Koerner, S.K.; Kolodziej, A.; Looby, R.J.; Sun, W.-C.; Zhang, Z. A lysine walk to high relaxivity collagen-targeted MRI contrast agents. *Chem. Commun.* **2009**, 430–432. [[CrossRef](#)] [[PubMed](#)]
34. Caravan, P.; Das, B.; Dumas, S.; Epstein, F.H.; Helm, P.A.; Jacques, V.; Koerner, S.; Kolodziej, A.; Shen, L.; Sun, W.C.; et al. Collagen-targeted MRI contrast agent for molecular imaging of fibrosis. *Angew. Chem. Int. Ed.* **2007**, *46*, 8171–8173. [[CrossRef](#)] [[PubMed](#)]
35. Wiethoff, A.J.; Barrett, J.A.; Wang, J.; Caravan, P.; Nair, S.; Melisi, M.A.; Williams, T.L.; Drzwecki, L.A.; Chesna, C.R.; Costello, C.R.; et al. Pharmacokinetics, biodistribution and efficacy of EP-1873: A Gd-based fibrin specific thrombus MR agent. *Proc. Int. Soc. Magn. Reson. Med.* **2003**, *11*, 833.
36. Overoye-Chan, K.; Koerner, S.; Looby, R.J.; Kolodziej, A.F.; Zech, S.G.; Deng, Q.; Chasse, J.M.; McMurry, T.J.; Caravan, P. EP-2104R: A Fibrin-Specific Gadolinium-Based MRI Contrast Agent for Detection of Thrombus. *J. Am. Chem. Soc.* **2008**, *130*, 6025–6039. [[CrossRef](#)]
37. Oliveira, B.L.; Caravan, P. Peptide-based fibrin-targeting probes for thrombus imaging. *Dalton Trans.* **2017**, *46*, 14488–14508. [[CrossRef](#)]
38. Spuentrup, E.; Botnar, R.M.; Wiethoff, A.J.; Ibrahim, T.; Kelle, S.; Katoh, M.; Özgun, M.; Nagel, E.; Vymazal, J.; Graham, P.B.; et al. MR imaging of thrombi using EP-2104R, a fibrin-specific contrast agent: Initial results in patients. *Eur. Radiol.* **2008**, *18*, 1995–2005. [[CrossRef](#)]
39. Ye, F.; Jeong, E.-K.; Jia, Z.; Yang, T.; Parker, D.; Lu, Z.-R. A Peptide Targeted Contrast Agent Specific to Fibrin-Fibronectin Complexes for Cancer Molecular Imaging with MRI. *Bioconjug. Chem.* **2008**, *19*, 2300–2303. [[CrossRef](#)]
40. Tripepi, M.; Capuana, F.; Gianolio, E.; Kock, F.V.C.; Pagoto, A.; Stefania, R.; Digilio, G.; Aime, S. Synthesis of High Relaxivity Gadolinium AAZTA Tetramers as Building Blocks for Bioconjugation. *Bioconjug. Chem.* **2018**, *29*, 1428–1437. [[CrossRef](#)]
41. Li, Y.; Han, Z.; Roelle, S.; DeSanto, A.; Sabatelle, R.; Schur, R.; Lu, Z.-R. Synthesis and Assessment of Peptide Gd-DOTA Conjugates Targeting Extradomain B Fibronectin for Magnetic Resonance Molecular Imaging of Prostate Cancer. *Mol. Pharmacol.* **2017**, *14*, 3906–3915. [[CrossRef](#)]

42. Ayat, N.R.; Qin, J.-C.; Cheng, H.; Roelle, S.; Gao, S.; Li, Y.; Lu, Z.-R. Optimization of ZD2 Peptide Targeted Gd(HP-DO3A) for Detection and Risk-Stratification of Prostate Cancer with MRI. *ACS Med. Chem. Lett.* **2018**, *9*, 730–735. [[CrossRef](#)] [[PubMed](#)]
43. Han, Z.; Li, Y.; Roelle, S.; Zhou, Z.; Liu, Y.; Sabatelle, R.; DeSanto, A.; Yu, X.; Zhu, H.; Magi-Galluzzi, C.; et al. Targeted Contrast Agent Specific to an Oncoprotein in Tumor Microenvironment with the Potential for Detection and Risk Stratification of Prostate Cancer with MRI. *Bioconjug. Chem.* **2017**, *28*, 1031–1040. [[CrossRef](#)] [[PubMed](#)]
44. Li, S.; Jiang, J.; Zou, J.; Qiao, J.; Xue, S.; Wei, L.; Long, R.; Wang, L.; Castiblanco, A.; White, N.; et al. PEGylation of protein-based MRI contrast agents improves relaxivities and biocompatibilities. *J. Inorg. Biochem.* **2012**, *107*, 111–118. [[CrossRef](#)]
45. Qiao, J.; Xue, S.; Pu, F.; White, N.; Jiang, J.; Liu, Z.-R.; Yang, J.J. Molecular imaging of EGFR/HER2 cancer biomarkers by protein MRI contrast agents. *J. Biol. Inorg. Chem.* **2014**, *19*, 259–270. [[CrossRef](#)] [[PubMed](#)]
46. Xue, S.; Qiao, J.; Jiang, J.; Hubbard, K.; White, N.; Wei, L.; Li, S.; Liu, Z.-R.; Yang, J.J. Design of ProCAs (Protein-Based Gd³⁺ MRI Contrast Agents) with High Dose Efficiency and Capability for Molecular Imaging of Cancer Biomarkers. *Med. Res. Rev.* **2014**, *34*, 1070–1099. [[CrossRef](#)] [[PubMed](#)]
47. Burden-Gulley, S.M.; Gates, T.J.; Burgoyne, A.M.; Cutter, J.L.; Lodowski, D.T.; Robinson, S.; Sloan, A.E.; Miller, R.H.; Basilion, J.P.; Brady-Kalnay, S.M. A Novel Molecular Diagnostic of Glioblastomas: Detection of an Extracellular Fragment of Protein Tyrosine Phosphatase μ . *Neoplasia* **2010**, *12*, 305–316. [[CrossRef](#)] [[PubMed](#)]
48. Herrmann, K.; Johansen, M.L.; Craig, S.E.; Vincent, J.; Howell, M.; Gao, Y.; Lu, L.; Erokwu, B.; Agnes, R.S.; Lu, Z.-R.; et al. Molecular Imaging of Tumors Using a Quantitative T(1) Mapping Technique via Magnetic Resonance Imaging. *Diagnostics* **2015**, *5*, 318–332. [[CrossRef](#)]
49. Johansen, M.L.; Gao, Y.; Hutnick, M.A.; Craig, S.E.L.; Pokorski, J.K.; Flask, C.A.; Brady-Kalnay, S.M. Quantitative Molecular Imaging with a Single Gd-Based Contrast Agent Reveals Specific Tumor Binding and Retention in Vivo. *Anal. Chem.* **2017**, *89*, 5932–5939. [[CrossRef](#)]
50. Lacerda, S.; Morfin, J.F.; Geraldes, C.F.G.C.; Toth, E. Metal complexes for multimodal imaging of misfolded protein-related diseases. *Dalton Trans.* **2017**, *46*, 14461–14474. [[CrossRef](#)]
51. André, F.; Martins, D.M.D.; Morfin, J.-F.; Lacerda, S.; Laurents, D.V.; Tóth, É.; Carlos, F.G.C. Geraldes Interaction of PiB-Derivative Metal Complexes with Beta-Amyloid Peptides: Selective Recognition of the Aggregated Forms. *Chemistry* **2015**, *21*, 5413–5422. [[CrossRef](#)]
52. Martins, A.F.; Morfin, J.-F.; Kubíčková, A.; Kubíček, V.; Buron, F.; Suzenet, F.; Salerno, M.; Lazar, A.N.; Duyckaerts, C.; Arlicot, N.; et al. PiB-Conjugated, Metal-Based Imaging Probes: Multimodal Approaches for the Visualization of β -Amyloid Plaques. *ACS Med. Chem.* **2013**, *4*, 436–440. [[CrossRef](#)] [[PubMed](#)]
53. Cressier, D.; Dhilly, M.; Pham, T.T.C.; Fillesoye, F.; Gourand, F.; Maïza, A.; Martins, A.F.; Morfin, J.-F.; Geraldes, C.F.G.C.; Tóth, É.; Barré, L. Gallium-68 Complexes Conjugated to Pittsburgh Compound B: Radiolabeling and Biological Evaluation. *Mol. Imaging Biol.* **2016**, *18*, 334–343. [[CrossRef](#)] [[PubMed](#)]

